Supplement: Derivation of mode normalization and perturbation theory

Thomas Weiss, Martin Mesch, Martin Schäferling, Harald Giessen, Wolfgang Langbein, and Egor A. Muljarov.

May 11, 2016

We derive the correct analytical mode normalization for periodic structures at normal incidence and use it to approximate the dependence of the resonance shift on the refractive index in a sensing volume by first-order perturbation theory derived from the resonant state expansion. Furthermore, we show how to calculate optical resonances from the scattering matrix efficiently, and discuss in detail our results for an array of rod antennas.

1 Periodic systems

1.1 Wave equation

This section is devoted to review Maxwell's equations in linear media and the derivation of the wave equation. The curl Maxwell's equations in cgs units and in frequency domain are as follows:

$$\nabla \times \mathbf{E} = ik_0\mu\mathbf{H}\,, \qquad \nabla \times \mathbf{H} = -ik_0\varepsilon\mathbf{E} + \frac{4\pi}{c}\mathbf{j}\,. \tag{S1}$$

In these equations and the following sections, a time dependence $\exp(-i\omega t)$ is assumed, and $k_0 = \omega/c$ is the vacuum wavenumber. Applying the curl operator to the first equation results for $\mu = 1$ in the following wave equation:

$$\mathcal{L}(\omega)\mathbf{E} \equiv -\nabla \times \nabla \times \mathbf{E} + k_0^2\varepsilon\mathbf{E} = -ik_0\frac{4\pi}{c}\mathbf{j}\,. \tag{S2}$$

We introduced here the operator $\mathcal{L}$ denoting the differential operator of the wave equation as a function of frequency ω.

1.2 Bloch's theorem

For periodic systems, we may use Bloch's theorem, and define $\mathbf{k}$ dependent electric and magnetic fields as well as currents as

$$\mathbf{E}(\mathbf{k},\mathbf{r}) = \mathrm{e}^{i\mathbf{k}\cdot\mathbf{r}}\mathbf{E}_\mathbf{k}(\mathbf{r})\,, \tag{S3a}$$

$$\mathbf{H}(\mathbf{k},\mathbf{r}) = \mathrm{e}^{i\mathbf{k}\cdot\mathbf{r}}\mathbf{H}_\mathbf{k}(\mathbf{r})\,, \tag{S3b}$$

$$\mathbf{j}(\mathbf{k},\mathbf{r}) = \mathrm{e}^{i\mathbf{k}\cdot\mathbf{r}}\mathbf{j}_\mathbf{k}(\mathbf{r})\,. \tag{S3c}$$

In this case, the wave vector $\mathbf{k}$ resides in the first Brillouin zone, and $\mathbf{E}_\mathbf{k}$, $\mathbf{H}_\mathbf{k}$, and $\mathbf{j}_\mathbf{k}$ denote functions depending on $\mathbf{k}$ and having the periodicity of the system. For the sake of simplicity and due to its high relevance, we will consider below only the case $\mathbf{k} = 0$, which corresponds to normal incidence. The more general case with arbitrary $\mathbf{k}$ will be discussed in future work. Henceforth, we will omit the subscript $\mathbf{k}$.

1.3 Reciprocal lattice

If we consider periodic systems, the permittivity obeys the following relation:

$$\varepsilon(\mathbf{r}+\mathbf{A})=\varepsilon(\mathbf{r})\,. \tag{S4}$$

In the two-dimensional periodic case, the vector $\mathbf{A}$ can be defined as $\mathbf{A}=A_1\mathbf{a}_1+A_2\mathbf{a}_2$, with A_α being integer multiples of the period P_α in direction α, and $\mathbf{a}_\alpha$ denoting a normalized basis vector in the direction of periodicity. Without the loss of generality, we assume $\mathbf{a}_1$ and $\mathbf{a}_2$ to be vectors perpendicular to the z axis. Note that, in general, the directions of periodicity can be non-orthogonal, i.e., $\mathbf{a}_\alpha\cdot\mathbf{a}_\beta\neq\delta_{\alpha\beta}$. For such a two-dimensional lattice, there exists a reciprocal lattice with reciprocal lattice vectors $\mathbf{G}=G_1\mathbf{g}_1+G_2\mathbf{g}_2$, where $G_\alpha=2\pi g_\alpha/P_\alpha$ for $g_\alpha\in\mathbb{Z}$. In this case, the normalized basis vectors $\mathbf{g}_\alpha$ fulfill the relation $\mathbf{g}_\alpha\cdot\mathbf{a}_\beta=\delta_{\alpha\beta}$.

1.4 Homogeneous layers

In the case that ε is isotropic and spatially independent in a slab or half-space, we can derive a general solution of equation (S2) in that region by a decomposition in plane waves. In a periodic system,

$$\mathbf{E}_{\mathrm{hom}}(\mathbf{r};\omega)=\sum_{\mathbf{G},p}a_{\mathbf{G}}^{(p)}(\omega)\mathbf{E}_{\mathbf{G}}^{(p)}(\omega)\mathrm{e}^{i\mathbf{G}\cdot\mathbf{r}+i\kappa_{\mathbf{G}}(\omega)z}\,, \tag{S5}$$

where $\mathbf{G}$ denotes reciprocal lattice vectors. The vector $\mathbf{E}_{\mathbf{G}}^{(p)}$ defines the polarization state and is independent of $\mathbf{r}$. There are two orthogonal polarization states for each $\mathbf{G}$, indicated by the superscript p. The orthogonal polarization basis can be chosen linearly (i.e., s for *senkrecht* and p for *parallel*) polarized, which we will do in the following. The polarization vector for a given $\mathbf{G}$ must satisfy the divergence equation:

$$\nabla\cdot\mathbf{E}_{\mathbf{G}}^{(p)}\mathrm{e}^{i\mathbf{G}\cdot\mathbf{r}+i\kappa_{\mathbf{G}}z}=0\,. \tag{S6}$$

While the lateral wave vector components $\mathbf{G}$ of the plane wave solutions can be considered as a set of parameters, the z component directly follows from equation (S2) for $\mathbf{j}=0$:

$$\kappa_{\mathbf{G}}=\pm\sqrt{\varepsilon k_0^2-\mathbf{G}^2}\,. \tag{S7}$$

The sign before the square root depends on the direction of propagation or decay of the corresponding solution of Maxwell's equations.

In the next sections, we will use the following orthogonality relation for linearly polarized solutions in homogeneous space. Integrating over one unit cell $\mathcal{U}$ with area S_{u} straightforwardly results in

$$\int_{\mathcal{U}}\mathrm{d}x\mathrm{d}y\,\mathbf{E}_{\mathbf{G}}^{(p)}\cdot\mathbf{E}_{\mathbf{G}'}^{(p')}\,\mathrm{e}^{i\mathbf{G}\cdot\mathbf{r}}\mathrm{e}^{i\mathbf{G}'\cdot\mathbf{r}}=S_{\mathrm{u}}\mathbf{E}_{\mathbf{G}}^{(p)}\cdot\mathbf{E}_{\mathbf{G}'}^{(p')}\delta_{\mathbf{G},-\mathbf{G}'}\delta_{p,p'}\,. \tag{S8}$$

2 Eigenstates and their normalization

It has been shown for single spherical particles and cylindrical structures as well as homogeneous waveguide layers [1–6] how the Green's dyadic of $\mathcal{L}$ can be expanded in terms of eigenstates $\mathbf{E}_m$ with complex eigenfrequencies ω_m, which for outgoing boundary conditions satisfy

$$\mathcal{L}(\omega_m)\mathbf{E}_m=0\,. \tag{S9}$$

For this purpose, a method has been developed to assign the proper weight to each eigenfunction, i.e., to carry out a correct mode normalization. In contrast to other methods [7–9],

the approach is fully analytical and does not involve any far-field approximations. Here, we extend this method to periodic systems.

The Green's dyadic of a periodic system satisfies the following equation:

$$\mathcal{L}(\omega)\mathcal{G}(\mathbf{r},\mathbf{r}';\omega) = \sum_{\mathbf{A}} \hat{1}\delta(\mathbf{r}-\mathbf{r}'-\mathbf{A})\,. \tag{S10}$$

The summation on the right hand side is understood to run over all lattice vectors $\mathbf{A}$. In order to expand the Green's dyadic in terms of eigenstates, we may first make an analytical continuation to the complex ω plane, on which the eigenstates denote a countable number of simple poles of $\mathcal{G}$. Except for the poles, the Green's dyadic remains finite over the whole complex frequency plane and vanishes for $|\omega| \to \infty$ when limiting the spatial regions to the periodic structure [1], i.e., when excluding homogenous layers on top and on bottom of a periodic stack of layers, where the fields can diverge for $|\omega| \to \infty$ due to the outgoing boundary conditions. We will focus now on such inner regions, including the interfaces to the outer homogeneous half-spaces. In contrast to aperiodic systems, the Green's dyadic exhibits discontinuities due to the Rayleigh anomalies [5]. Hence, in combination with the Mittag-Leffler theorem [10], we can expand the Green's dyadic locally as

$$\mathcal{G}(\mathbf{r},\mathbf{r}';\omega) = \sum_{m} \frac{\mathcal{R}_m(\mathbf{r},\mathbf{r}')}{\omega-\omega_m} + \Delta\mathcal{G}(\mathbf{r},\mathbf{r}';\omega)\,, \tag{S11}$$

where $\mathcal{R}$ is a tensor that has yet to be determined, and the influence of the Rayleigh anomaly can be written as [5]

$$\Delta\mathcal{G}(\mathbf{r},\mathbf{r}';\omega) = \frac{1}{2\pi i}\sum_{m} \int_{-\infty}^{0} \mathrm{d}\zeta\, \frac{\Delta\mathcal{G}_m(\mathbf{r},\mathbf{r}';\zeta)}{\omega-c_m-i\zeta}\,, \tag{S12}$$

with $\Delta\mathcal{G}_m(\mathbf{r},\mathbf{r}';\zeta) = \lim_{\delta\to 0}\mathcal{G}(\mathbf{r},\mathbf{r}';c_m+\delta+i\zeta) - \mathcal{G}(\mathbf{r},\mathbf{r}';c_m-\delta+i\zeta)$. Here, c_m denotes branch points due to the Rayleigh anomalies on the real frequency axis.

We proceed as in [3, 4, 6] and introduce an analytical continuation $\tilde{\mathbf{E}}_m(\mathbf{r};\omega)$ of $\mathbf{E}_m(\mathbf{r})$ around ω_m with

$$\lim_{\omega\to\omega_m} \tilde{\mathbf{E}}_m(\mathbf{r};\omega) = \mathbf{E}_m(\mathbf{r})\,, \tag{S13}$$

which is defined as a solution of the following differential equation:

$$\mathcal{L}(\omega)\tilde{\mathbf{E}}_m(\mathbf{r},\omega) = \frac{\omega^2-\omega_m^2}{c^2}\sigma_m(\mathbf{r})\,. \tag{S14}$$

In this case, $\sigma_m(\mathbf{r})$ is an arbitrary periodic source vanishing outside the periodic structure.

The solution of equation (S14) can be obtained by convoluting the Green's dyadic with the source term. Using our ansatz defined in equation (S11), we obtain:

$$\begin{aligned}\tilde{\mathbf{E}}_m(\mathbf{r};\omega) = &\sum_{m'} \frac{1}{c^2}\frac{\omega^2-\omega_m^2}{\omega-\omega_{m'}} \int_{\mathcal{V}} \mathrm{d}V' \mathcal{R}_{m'}(\mathbf{r},\mathbf{r}')\cdot\sigma_m(\mathbf{r}') \\ &+ \sum_{m'} \frac{\omega^2-\omega_m^2}{2\pi i c^2} \int_{c_m-i\infty}^{c_m} \mathrm{d}\omega' \int_{\mathcal{V}} \mathrm{d}V' \frac{\Delta\mathcal{G}_{m'}(\mathbf{r},\mathbf{r}';\omega')}{\omega-\omega'}\cdot\sigma_m(\mathbf{r}')\,.\end{aligned} \tag{S15}$$

Taking the limit $\omega \to \omega_m$, it is obvious that all terms with $\omega_{m'} \neq \omega_m$ as well as all contributions from the Rayleigh anomalies will vanish. Therefore, the integral in the first line of equation (S15) must result for $m = m'$ in a term proportional to $\mathbf{E}_m$, leading to the following ansatz for $\mathcal{R}_m$:

$$\mathcal{R}_m(\mathbf{r},\mathbf{r}') = c^2 \frac{\mathbf{E}_m(\mathbf{r})\otimes\mathbf{F}_m(\mathbf{r}')}{2\omega_m}\,. \tag{S16}$$

This ansatz requires that

$$\int_{\mathcal{V}} \mathrm{d}V\, \mathbf{F}_m(\mathbf{r}) \cdot \sigma_m(\mathbf{r}) = 1\,, \tag{S17}$$

where $\mathcal{V}$ is a volume limited to one unit cell in the periodic directions and sufficiently large to include all non-zero regions of σ_m in the aperiodic directions. The symbol $\otimes$ denotes the vector direct product. The relation is not valid for poles at $\omega = 0$, i.e., static modes, which are necessary for a complete set of resonant states, but can be omitted for the perturbation theory that we develop here.

In the case that two modes are degenerate, we may chose appropriate source terms σ_m, which ensure that $\int_{\mathcal{V}} \mathrm{d}V\, \mathbf{F}_m(\mathbf{r}) \cdot \sigma_{m'}(\mathbf{r}) = \delta_{mm'}$ for the degenerate modes. Furthermore, considering reciprocity, it directly follows that $\mathbf{F}_m = \mathbf{E}_m$. In summary, the general eigentstate decomposition of the Green's dyadic yields for reciprocal periodic systems at normal incidence

$$\mathcal{G}(\mathbf{r}, \mathbf{r}'; \omega) = c^2 \sum_m \frac{\mathbf{E}_m(\mathbf{r}) \otimes \mathbf{E}_m(\mathbf{r}')}{2\omega_m\,(\omega - \omega_m)} + \Delta\mathcal{G}(\mathbf{r}, \mathbf{r}'; \omega)\,. \tag{S18}$$

We can now derive the proper normalization of the modes by following the procedure described in [1–6]. Let us consider equation (S14) and expand the differential equation for small deviations from ω_m using $\omega = \omega_m + \Delta\omega$. Thus, the differential equation yields:

$$\begin{aligned} \frac{2\omega_m}{c^2}\Delta\omega\sigma_m + \frac{\Delta\omega^2}{c^2}\sigma_m = &-\nabla\times\nabla\times\left[\mathbf{E}_m + \tilde{\mathbf{E}}'_m\Delta\omega + \mathcal{O}(\Delta\omega^2)\right] + \\ &+ \left[\frac{\omega_m^2}{c^2}\varepsilon(\mathbf{r};\omega_m) + \frac{\partial\left(\omega^2\varepsilon\right)}{c^2\partial\omega}\bigg|_{\omega_m}\Delta\omega + \mathcal{O}(\Delta\omega^2)\right]\left[\mathbf{E}_m + \tilde{\mathbf{E}}'_m\Delta\omega + \mathcal{O}(\Delta\omega^2)\right]. \end{aligned} \tag{S19}$$

Note that we have used equation (S13) to evaluate the zeroth order of the Taylor expansion of $\tilde{\mathbf{E}}_m$, while $\tilde{\mathbf{E}}'_m$ denotes the first order derivative of $\tilde{\mathbf{E}}_m$ with respect to ω at ω_m. Sorting this equation by powers of $\Delta\omega$ up to linear order results in the following independent equations:

$$-\nabla\times\nabla\times\mathbf{E}_m + \frac{\omega_m^2}{c^2}\varepsilon(\mathbf{r};\omega_m)\mathbf{E}_m = 0\,, \tag{S20}$$

$$-\nabla\times\nabla\times\tilde{\mathbf{E}}'_m + \frac{\omega_m^2}{c^2}\varepsilon(\mathbf{r};\omega_m)\tilde{\mathbf{E}}'_m + \frac{\partial\left(\omega^2\varepsilon\right)}{c^2\partial\omega}\bigg|_{\omega_m}\mathbf{E}_m = \frac{2\omega_m}{c^2}\sigma_m\,. \tag{S21}$$

The first equation is simply the eigenvalue equation for $\mathbf{E}_m$ and ω_m. Multiplying the second equation from the left with $\mathbf{E}_m$ and the first equation with $\tilde{\mathbf{E}}'_m$ and subtracting one from the other results in

$$-\mathbf{E}_m\cdot\left(\nabla\times\nabla\times\tilde{\mathbf{E}}'_m\right) + \tilde{\mathbf{E}}'_m\cdot(\nabla\times\nabla\times\mathbf{E}_m) + \mathbf{E}_m\cdot\frac{\partial\left(\omega^2\varepsilon\right)}{c^2\partial\omega}\bigg|_{\omega_m}\mathbf{E}_m = \frac{2\omega_m}{c^2}\mathbf{E}_m\cdot\sigma_m\,. \tag{S22}$$

Integration over a volume $\mathcal{V}$ large enough to span over one unit cell as well as the whole structure of interest yields in combination with equation (S17):

$$\frac{c^2}{2\omega_m}\int_{\mathcal{V}}\mathrm{d}V\left[-\mathbf{E}_m\cdot\left(\nabla\times\nabla\times\tilde{\mathbf{E}}'_m\right) + \tilde{\mathbf{E}}'_m\cdot(\nabla\times\nabla\times\mathbf{E}_m) + \mathbf{E}_m\cdot\frac{\partial\left(\omega^2\varepsilon\right)}{c^2\partial\omega}\bigg|_{\omega_m}\mathbf{E}_m\right] = 1\,. \tag{S23}$$

In the third term of the integral, the derivative of $\omega^2\varepsilon$ with respect to ω can be transformed into a derivative with respect to ω^2 to absorb the prefactor $c^2/2\omega_m$. The first two terms can be converted into a surface integral using vector identities. In combination with the divergence condition of the electric field in homogeneous space, we thus obtain the normalization condition

$$I_m + S_m = 1\,, \tag{S24}$$

where the contributions I_m and S_m are given by

$$I_m = \int_{\mathcal{V}} \mathrm{d}V\, \mathbf{E}_m \cdot \left.\frac{\partial(\omega^2\varepsilon)}{\partial(\omega^2)}\right|_{\omega_m} \mathbf{E}_m\,, \tag{S25}$$

$$S_m = \frac{c^2}{2\omega_m} \oint_{\partial\mathcal{V}} \mathrm{d}S \left(\mathbf{E}_m \cdot \partial_s \tilde{\mathbf{E}}'_m - \tilde{\mathbf{E}}'_m \cdot \partial_s \mathbf{E}_m\right). \tag{S26}$$

Here, $\partial\mathcal{V}$ denotes the surface of $\mathcal{V}$, and ∂_s is the derivative in the direction of the surface normal. A great simplification occurs due to $\mathcal{V}$ spanning over one unit cell, because in this case, the surface integral vanishes in all periodic directions. Thus, for periodic stacks of layers, we only have to deal with the top and bottom surfaces in the superstrate and substrate, respectively.

Equation (S26) contains the yet unknown $\tilde{\mathbf{E}}'_m$. As the non-vanishing aperiodic contributions of surface ∂V are in the exterior regions of our system, where $\tilde{\mathbf{E}}_m$ is a solution of homogeneous space that obeys the continuity conditions at the outermost interfaces as well as outgoing boundary conditions to the far field, we can decompose it in the outer regions (denoted by $\mathbf{r}_>$) into a plane wave basis:

$$\tilde{\mathbf{E}}_m(\mathbf{r}^\nu_>;\omega) = \sum_{\mathbf{G},p} \underbrace{\tilde{a}^{(p,\nu)}_{m,\mathbf{G}}(\omega)\mathbf{E}^{(p,\nu)}_{\mathbf{G}}(\omega)}_{\equiv \mathbf{E}^{(p,\nu)}_{m,\mathbf{G}}(\omega)} \underbrace{\mathrm{e}^{i\mathbf{G}\cdot\mathbf{r}^\nu_> + i\kappa^\nu_{\mathbf{G}}(\omega)\Delta z}}_{\equiv \psi^\nu_{\mathbf{G}}(\mathbf{r}^\nu_>;\omega)}. \tag{S27}$$

By Δz, we denote here the distance to the plane, on which the expansion coefficients $\tilde{a}^{(p,\nu)}_{m,\mathbf{G}}$ are defined, with $\Delta z > 0$ specifying points in space that are further away from the periodic structure. The superscript ν indicates whether we consider the expansion in the top or bottom half-space. The frequency-dependent polarization vectors $\mathbf{E}^{(p,\nu)}_{\mathbf{G}}$ are normalized such that

$$S_{\mathrm{u}}\mathbf{E}^{(p,\nu)}_{\mathbf{G}}(\omega_m) \cdot \mathbf{E}^{(p,\nu)}_{-\mathbf{G}}(\omega_m) = 1\,. \tag{S28}$$

Note that the frequency dependence of the polarization vector $\mathbf{E}^{(p,\nu)}_{\mathbf{G}}$ in equation (S27) follows from equation (S6) and the frequency dependence of $\kappa^\nu_{\mathbf{G}}$ for a non-vanishing z component of $\mathbf{E}^{(p,\nu)}_{\mathbf{G}}$. Therefore, in p polarization, we have to account for the frequency dependence, while in s polarization, we can choose $\mathbf{E}^{(\mathrm{s},\nu)}_{\mathbf{G}}$ such that it does not depend on ω due to its zero z component.

From equation (S27), we can now derive $\tilde{\mathbf{E}}'_m$ by differentiating with respect to ω at ω_m:

$$\tilde{\mathbf{E}}'_m = \sum_{\mathbf{G},p} \left.\frac{\partial \mathbf{E}^{(p,\nu)}_{m,\mathbf{G}}}{\partial\omega}\right|_{\omega_m} \psi^\nu_{\mathbf{G}}(\mathbf{r}^\nu_>;\omega_m) + \mathbf{E}^{(p,\nu)}_{m,\mathbf{G}}(\omega_m) \left.\frac{\partial\psi^\nu_{\mathbf{G}}}{\partial\omega}\right|_{\omega_m}. \tag{S29}$$

As $\mathbf{E}^{(p,\nu)}_{m,\mathbf{G}}$ is independent of $\mathbf{r}^\nu_>$, the integrand of the surface term in equation (S26) yields

$$\begin{aligned}\mathbf{E}_m \cdot \partial_s \tilde{\mathbf{E}}'_m - \tilde{\mathbf{E}}'_m \cdot \partial_s \mathbf{E}_m = \sum_{\mathbf{G},\mathbf{G}',p,p'} & \mathbf{E}^{(p,\nu)}_{m,\mathbf{G}}(\omega_m) \cdot \left.\frac{\partial \mathbf{E}^{(p',\nu)}_{m,\mathbf{G}'}}{\partial\omega}\right|_{\omega_m} \left(\psi^\nu_{\mathbf{G}} \frac{\partial\psi^\nu_{\mathbf{G}'}}{\partial s} - \psi^\nu_{\mathbf{G}'} \frac{\partial\psi^\nu_{\mathbf{G}}}{\partial s}\right) \\ & + \mathbf{E}^{(p,\nu)}_{m,\mathbf{G}}(\omega_m) \cdot \mathbf{E}^{(p',\nu)}_{m,\mathbf{G}'}(\omega_m) \left(\psi^\nu_{\mathbf{G}} \left.\frac{\partial^2\psi^\nu_{\mathbf{G}'}}{\partial s \partial\omega}\right|_{\omega_m} - \frac{\partial\psi^\nu_{\mathbf{G}}}{\partial s} \left.\frac{\partial\psi^\nu_{\mathbf{G}'}}{\partial\omega}\right|_{\omega_m}\right).\end{aligned} \tag{S30}$$

If we assume that the outermost surface of the normalization volume towards the upper and lower half-spaces is a plane normal to the z direction, then we can use the orthogonality relation defined in equation (S8) to simplify the evaluation of the surface integration in

equation (S26). Let $\mathcal{S}^\nu$ be the surface to the top and bottom half-spaces. Then, due to $\kappa^\nu_{\mathbf{G}} = \kappa^\nu_{-\mathbf{G}}$ as well as the orthogonality of plane waves,

$$\begin{aligned}\int\limits_{\mathcal{S}^\nu} \mathrm{d}S \left(\psi^\nu_{\mathbf{G}} \frac{\partial \psi^\nu_{\mathbf{G}'}}{\partial s} - \psi^\nu_{\mathbf{G}'} \frac{\partial \psi^\nu_{\mathbf{G}}}{\partial s}\right) &= i[\kappa^\nu_{\mathbf{G}}(\omega_m) - \kappa^\nu_{\mathbf{G}'}(\omega_m)] \int\limits_{\mathcal{S}^\nu} \mathrm{d}S \psi^\nu_{\mathbf{G}} \psi^\nu_{\mathbf{G}'} \\ &= i[\kappa^\nu_{\mathbf{G}}(\omega_m) - \kappa^\nu_{\mathbf{G}'}(\omega_m)] S_\mathrm{u} \delta_{\mathrm{G},-\mathrm{G}'} = 0\,,\end{aligned} \tag{S31}$$

and

$$\begin{aligned}&\int\limits_{\mathcal{S}^\nu} \mathrm{d}S \left(\psi^\nu_{\mathbf{G}} \frac{\partial^2 \psi^\nu_{\mathbf{G}'}}{\partial s \partial \omega}\bigg|_{\omega_m} - \frac{\partial \psi^\nu_{\mathbf{G}}}{\partial s} \frac{\partial \psi^\nu_{\mathbf{G}'}}{\partial \omega}\bigg|_{\omega_m}\right) = \\ &= \int\limits_{\mathcal{S}^\nu} \mathrm{d}S \psi^\nu_{\mathbf{G}} \psi^\nu_{\mathbf{G}'} \left(i \frac{\partial \kappa^\nu_{\mathbf{G}'}}{\partial \omega}\bigg|_{\omega_m} - \Delta z \kappa_{\mathbf{G}'} \frac{\partial \kappa^\nu_{\mathbf{G}'}}{\partial \omega}\bigg|_{\omega_m} + \Delta z \kappa_{\mathbf{G}} \frac{\partial \kappa^\nu_{\mathbf{G}'}}{\partial \omega}\bigg|_{\omega_m}\right) = i S_\mathrm{u} \frac{\partial \kappa^\nu_{\mathbf{G}}}{\partial \omega}\bigg|_{\omega_m} \delta_{\mathrm{G},-\mathrm{G}'}\,,\end{aligned} \tag{S32}$$

so that we obtain:

$$S^\nu_m \equiv \frac{c^2}{2\omega_m} \int\limits_{\mathcal{S}^\nu} \mathrm{d}S \left(\mathbf{E}_m \cdot \partial_s \tilde{\mathbf{E}}'_m - \tilde{\mathbf{E}}'_m \cdot \partial_s \mathbf{E}_m\right) = \frac{ic^2}{2\omega_m} \sum_{\mathbf{G},p} \frac{\partial \kappa^\nu_{\mathbf{G}}}{\partial \omega}\bigg|_{\omega_m} a^{(p,\nu)}_{m,-\mathbf{G}} a^{(p,\nu)}_{m,\mathbf{G}}\,. \tag{S33}$$

Here, we have introduced the abbreviation $a^{(p,\nu)}_{m,\mathbf{G}} \equiv \tilde{a}^{(p,\nu)}_{m,\mathbf{G}}(\omega_m)$. Thus, in summary,

$$S_m = S^\mathrm{top}_m + S^\mathrm{bot}_m\,, \tag{S34}$$

where the superscripts denote the corresponding contributions from the top and bottom half-spaces, respectively.

Note that using equation (S7) for calculating the derivative of $\kappa^\nu_{\mathbf{G}}$ with respect to ω, it is straight-forward to obtain equation (5) of the main manuscript from equation (S33) and to also show that for evanescently decaying channels, the normalization via finite volume and surface term is equivalent to a normalization by evaluating the volume integral over the whole space without any surface term.

In numerical calculations, the normalization according to equation (S24), with volume and surface terms defined by equations (S25) and (S34), can be carried out with the help of the orthogonality relation (S8). This relation allows to calculate the plane wave expansion on the outer surface of $\mathcal{V}$. In the case of the Fourier modal method [11, 12], which we used here, the expansion coefficient for the surface term (S34) can be even derived as a direct output of the calculation, so that one only has to evaluate the volume term (S25) by numerical integration to obtain the correct analytical mode normalization.

3 Generalization of the normalization condition

So far, we have assumed a special outermost surface that is a plane normal to the z axis. However, it is straight-forward to show that the normalization can be carried out for any arbitrarily shaped outer surface that spans over one unit cell and covers a finite volume of normalization. For this purpose, consider equation (S22) and integrate it over a volume $\mathcal{V}_\mathrm{h}$ that is completely located in the exterior homogeneous space, where $\sigma_m = 0$. We can then derive with some vector identities:

$$I^\mathrm{h}_m \equiv \int\limits_{\mathcal{V}_\mathrm{h}} \mathrm{d}V\, \mathbf{E}_m \cdot \frac{\partial(\omega^2 \varepsilon)}{\partial(\omega^2)}\bigg|_{\omega_m} \mathbf{E}_m = -\frac{c^2}{2\omega_m} \oint\limits_{\partial \mathcal{V}_\mathrm{h}} \mathrm{d}S \left(\mathbf{E}_m \cdot \partial_s \tilde{\mathbf{E}}'_m - \tilde{\mathbf{E}}'_m \cdot \partial_s \mathbf{E}_m\right)\,. \tag{S35}$$

We will now assume that $\partial\mathcal{V}_\mathrm{h}$ is composed of a flat surface $\partial\mathcal{V}_z$ that is a plane normal to the z axis, as well as some remaining surface $\partial\mathcal{V}'$. The remaining surface consists of the boundaries of one unit cell as well as an arbitrarily shaped surface $\mathcal{S}'$ to the exterior regions. For the flat surface, we have shown above that the surface integral over one unit cell results in equation (S33). Furthermore, due to periodicity, all contributions to $\partial\mathcal{V}'$ that belong to the boundaries of the unit cell cancel out each other. Accounting for the direction of the surface normals, we deduce that

$$I_m^\mathrm{h} = S_m^\nu - S'_m\,, \tag{S36}$$

where S'_m is the surface integral over the surface $\mathcal{S}'$. Equation (S36) thus provides a relation for the contribution of an arbitrary surface using that of a known flat surface S_m^ν as well as the integral I_m^h over the part of the volume that is bound between these surfaces while spanning over one unit cell. Inserting S_m^ν from equation (S36) in equations (S34) and (S24), we see that I_m^h accounts for the deviation in the normalization volume, while S'_m provides the modified surface contribution.

Furthermore, when substituting $\mathbf{E}_m$ in the volume term I_m^h by $\tilde{\mathbf{E}}_m(\mathbf{r}_>^\nu;\omega_m)$ as defined in equation (S27), we deduce from equation (S36) in combination with equation (S33) that the surface contribution S'_m only depends on the known modal expansion of the fields, which is given by the expansion coefficients $a_{m,\mathbf{G}}^{(p,\nu)}$. This is a non-trivial finding, as $\tilde{\mathbf{E}}'_m$ might possess some additional contributions that depend on the actual choice of σ_m. In equation (S27), such additional contributions are present due to the frequency dependence of $\tilde{a}_{m,\mathbf{G}}^{(p,\nu)}$ and enter the surface integral in equation (S26) in form of the first-order frequency derivative evaluated at ω_m. However, when calculating S'_m on an arbitrary surface spanning over one unit cell, we see that the surface integral with the additional contributions must equal zero.

This can be also shown in a direct manner due to the fact that, in the exterior, the additional contributions appear as a linear combination of plane waves that are solutions of the source-free wave equation in homogeneous space. If $\mathbf{E}_A$ and $\mathbf{E}_B$ denote two solutions of the wave equation in the exterior homogeneous space, then the following relation holds in the exterior:

$$\mathbf{E}_A\cdot\mathcal{L}(\omega)\mathbf{E}_B - \mathbf{E}_A\cdot\mathcal{L}(\omega)\mathbf{E}_B = -\mathbf{E}_A\cdot(\nabla\times\nabla\times\mathbf{E}_B) + \mathbf{E}_B\cdot(\nabla\times\nabla\times\mathbf{E}_A) = 0\,. \tag{S37}$$

Integrating this equation over a volume in homogeneous space, and using the same vector identities as in the derivation of equation (S26), we see that, on the one hand, for any closed surface in homogeneous space,

$$\oint \mathrm{d}S(\mathbf{E}_A\cdot\partial_s\mathbf{E}_B - \mathbf{E}_B\cdot\partial_s\mathbf{E}_A) = 0\,. \tag{S38}$$

On the other hand, from equation (S31), we can now deduce that integrating the same function only over a plane normal to the z axis equals zero as well. Consequently, for the closed surface $\partial\mathcal{V}_\mathrm{h}$ that is composed of such a plane as well as the boundaries of the unit cell and a remaining surface $\mathcal{S}'$, we see that the surface integral over $\mathcal{S}'$ must vanish.

Hence, for the analytical continuation of the resonant field distribution $\mathbf{E}_m$ in the exterior homogeneous space, we can introduce the regularized field

$$\mathbf{E}_m^{(\mathrm{reg})}(\mathbf{r}_>^\nu;\omega) = \sum_{\mathbf{G},p} a_{m,\mathbf{G}}^{(p,\nu)}\mathbf{E}_\mathbf{G}^{(p,\nu)}(\omega_m)\,\mathrm{e}^{i\mathbf{G}\cdot\mathbf{r}_>^\nu + i\kappa_\mathbf{G}^\nu(\omega)\Delta z} \tag{S39}$$

when calculating $\tilde{\mathbf{E}}'_m$ in equation (S24). This regularized field only depends on the expansion coefficients $a_{m,\mathbf{G}}^{(p,\nu)}$ of the resonant fields, thus reducing the surface integral in equation (S26) to expressions that are based on the solution of equation (S9). Thus, we obtain the following

normalization condition:

$$1 = \underbrace{\int_{\mathcal{V}} \mathrm{d}V\, \mathbf{E}_m \cdot \left.\frac{\partial(\omega^2\varepsilon)}{\partial(\omega^2)}\right|_{\omega_m} \mathbf{E}_m}_{=I_m} + \underbrace{\frac{c^2}{2\omega_m} \oint_{\partial\mathcal{V}} \mathrm{d}S \left(\mathbf{E}_m \cdot \left.\frac{\partial^2 \mathbf{E}_m^{(\mathrm{reg})}}{\partial s \partial\omega}\right|_{\omega_m} - \left.\frac{\partial \mathbf{E}_m^{(\mathrm{reg})}}{\partial\omega}\right|_{\omega_m} \cdot \frac{\partial \mathbf{E}_m}{\partial s} \right)}_{=S_m}, \quad \text{(S40)}$$

where S_m immediately results in equation (S34) when using the expansion defined in equation (S39).

Let us now review the above derivations and examine their generality. First of all, equations (S24) to (S26) simply state that for any optical system, the normalization contains a volume and a surface contribution. This is always valid, independently of the underlying geometry. The periodic structure comes into play when evaluating the expansion of the fields in the exterior, see equation (S27). This results in the special form of the surface contributions given in equations (S33) and (S34). For other geometries as those described in [1–6], the final surface contribution in the analytical normalization relation might differ, but the principles of its derivation are the same and based on equations (S24) to (S26).

In the case of single particles, for instance, the outgoing solutions can be expanded in terms of vector spherical harmonics [13], for which the radial dependence of the fields can be separated as a function $f_\lambda(kr)$ with $k = \sqrt{\varepsilon}\omega/c$. As shown in [4], using that $\omega_m \partial_\omega f_\lambda(kr) = r\partial_r f_\lambda(kr)$ for a non-dispersive material in the exterior, we obtain the following analytical surface term:

$$S_m = \frac{c^2}{2\omega_m^2} \oint_{\partial\mathcal{V}} \mathrm{d}S \left(\mathbf{E}_m \cdot \frac{\partial}{\partial s} r \frac{\partial \mathbf{E}_m}{\partial r} - r \frac{\partial \mathbf{E}_m}{\partial r} \cdot \frac{\partial \mathbf{E}_m}{\partial s} \right). \quad \text{(S41)}$$

Here, as in the case of the periodic arrays, the starting point of the derivation is equation (S26). As equation (S26) contains $\tilde{\mathbf{E}}'_m$, which might have contributions that cannot be directly derived from the resonant field distribution $\mathbf{E}_m$, it is necessary to proof that these additional contributions provide a zero in the surface term. Above, the proof has been carried out exemplarily for one- and two-dimensional periodic arrays, with the result being summarized in equations (S39) and (S40), but the steps are the same for other geometries when using an appropriate set of basis states in the homogeneous exterior space, such as the vector spherical harmonics for single particles. Thus, one can define regularized fields that are based only on the resonant field distribution $\mathbf{E}_m$.

Compared to the periodic structures, the derivation of the mode normalization for spherical geometries (as well as for the homogeneous slabs and the cylindrical structures discussed in [3, 5]) with a non-dispersive material in the exterior is simplified due to the absence of Rayleigh anomalies as well as the fact that we can find a simple relation to transform the frequency derivative in equation (S26) into a spatial derivative. Therefore, the present derivation of the correct analytical mode normalization provides a non-trivial modification of the previous normalization procedures described in [1–6]. It is worth mentioning that the previous formulations already included dispersive materials, while the current formulation with equation (S34) additionally allows for considering lossless dispersive materials in the exterior domain (i.e., in the case that we are far enough away from poles in the material to neglect losses, but close enough so that dispersion is important).

4 Resonant state expansion

Let us now follow [1–5] in order to derive the resonant state expansion for a perturbed system of periodic nanoantennas, in which the permittivity deviates from the original one by a $\Delta\varepsilon(\mathbf{r};\omega)$. The modified system exhibits eigenstates $\mathbf{E}_\mu$ and eigenfrequencies ω_μ, which

obey the following differential equation:

$$\mathcal{L}_{\Delta\varepsilon}(\omega_\mu)\mathbf{E}_\mu = \left[\mathcal{L}(\omega_\mu) + \frac{\omega_\mu^2}{c^2}\Delta\varepsilon(\mathbf{r};\omega_\mu)\right]\mathbf{E}_\mu = 0\,. \tag{S42}$$

Next, we can expand the Green's dyadic of $\mathcal{L}$ in its eigenstates and understand $-\Delta\varepsilon(\mathbf{r};\omega_\mu)\mathbf{E}_\mu$ as a source term for the unperturbed wave equation. With the ansatz $\mathbf{E}_\mu = \sum_m b_m\mathbf{E}_m + \Delta\mathbf{E}_\mu$, where $\Delta\mathbf{E}_\mu$ accounts for the influence of the Rayleigh anomalies, it is thus possible to set up a system of equations that can be solved for the expansion coefficients b_m and resonance frequencies ω_μ. It is worth mentioning that using the Green's dyadic as defined in equation (S18), the system of equations depends in general non-linearly on ω_μ, so that the derivation of non-trivial solutions is rather complicated. In the standard formulation of the resonant state expansion [1–5], assuming non-dispersive materials, it is possible to reformulate the Green's dyadic using the sum rule $\sum_m \mathbf{E}_m(\mathbf{r})\otimes\mathbf{E}_m(\mathbf{r}')/\omega_m = 0$ in order to obtain a linear eigenvalue problem for eigenvalues ω_μ and eigenvectors consisting of the expansion coefficients b_m. For dispersive materials, this approach is no longer applicable. Recently, the formulation of the resonant state expansion has been extended to dispersive materials described by a Drude-Lorentz model [14]. Especially for large perturbations and in the case that the poles of the Drude-Lorentz model are close to resonances of our unperturbed system, such an extension is necessary to determine the resonances of the perturbed system correctly. However, for small perturbations, we may simply use the Green's dyadic of equation (S18), which yields:

$$\begin{aligned}\mathbf{E}_\mu = &\sum_m \mathbf{E}_m(\mathbf{r})\int_{\mathcal{V}} \mathrm{d}V' \frac{-\omega_\mu^2}{2\omega_m(\omega_\mu-\omega_m)}\mathbf{E}_m(\mathbf{r}')\cdot\Delta\varepsilon(\mathbf{r}';\omega_\mu)\mathbf{E}_\mu(\mathbf{r}')\\ &-\int_{\mathcal{V}} \mathrm{d}V'\Delta\mathcal{G}(\mathbf{r},\mathbf{r}';\omega_\mu)\frac{\omega_\mu^2}{c^2}\Delta\varepsilon(\mathbf{r}';\omega_\mu)\mathbf{E}_\mu(\mathbf{r}')\,.\end{aligned} \tag{S43}$$

Our goal is now to derive an equation valid to describe small perturbations, for which the eigenstates of the original system can be assumed also as the eigenstates of the perturbed system, i.e., $\mathbf{E}_\mu \approx \mathbf{E}_m$. Such an approximation is justified, whenever we expect small changes $\Delta\omega = \omega_\mu - \omega_m$ in resonance frequency and the criterion $\int_{\mathcal{V}} \mathrm{d}V\,\mathbf{E}_m\cdot\Delta\varepsilon\mathbf{E}_{m'}\,\omega_m/(\omega_m-\omega_{m'}) \ll 1$ is fulfilled $\forall\, m' \neq m$ in $\mathcal{V}$. This means that the applicability of the first-order perturbation theory has to be checked carefully in cases where we have close-by resonances or where we obtain huge resonant field enhancements in the unperturbed system, e.g., for gap antennas. Whenever the aforementioned criterion is fulfilled, equation (S43) simplifies to

$$2\omega_m(\omega_\mu-\omega_m) + \omega_\mu^2 I_m^{\mathcal{V}}[\Delta\varepsilon(\mathbf{r};\omega_\mu)] = 0\,, \tag{S44}$$

with

$$I_m^{\mathcal{V}}[\varphi(\mathbf{r};\omega)] = \int_{\mathcal{V}} \mathrm{d}V\mathbf{E}_m(\mathbf{r})\cdot\varphi(\mathbf{r};\omega)\mathbf{E}_m(\mathbf{r})\,, \tag{S45}$$

where φ is a placeholder for a tensor with a specific dependence on frequency and position. Equation (S44) is a transcendental equation for the approximate resonance frequency ω_μ of the perturbed system. Its solutions can be easily derived up to machine precision using standard numerical procedures such as the Newton method. In the case that $\Delta\varepsilon$ does not depend on frequency, we can even derive a closed expression for the approximate resonance frequency ω_μ:

$$\omega_\mu \approx \frac{\omega_m}{I_m^{\mathcal{V}}(\Delta\varepsilon)}\left(\sqrt{1+2I_m^{\mathcal{V}}(\Delta\varepsilon)}-1\right)\,. \tag{S46}$$

If the perturbation $\Delta\varepsilon$ depends only weakly on the frequency, it is also possible to derive a closed expression by using $\Delta\varepsilon(\mathbf{r};\omega) \approx \Delta\varepsilon(\mathbf{r};\omega_m) + \Delta\varepsilon'\Delta\omega$, where $\Delta\varepsilon'$ is the first order derivative of $\Delta\varepsilon$ with respect to ω evaluated at ω_m. Then, by neglecting all higher than linear orders in $\Delta\omega$, we can derive from equation (S44) that

$$\Delta\omega \approx \frac{-\omega_m I_m^{\mathcal{V}}[\Delta\varepsilon(\mathbf{r};\omega_m)]}{2 + 2I_m^{\mathcal{V}}[\Delta\varepsilon(\mathbf{r};\omega_m)] + I_m^{\mathcal{V}}(\Delta\varepsilon')\omega_m}\,. \tag{S47}$$

Considering that $\Delta\varepsilon$ is zero except for a volume $\mathcal{T}$, in which it should be a constant scalar, we obtain for $\Delta\varepsilon \to 0$ either from equation (S46) or (S47):

$$\frac{\partial\omega_m}{\partial\varepsilon} = -\frac{\omega_m}{2}\int\limits_{\mathcal{T}} \mathrm{d}V\mathbf{E}_m^2(\mathbf{r})\,. \tag{S48}$$

In this case, the derivative on the left hand side is understood at $\Delta\varepsilon = 0$, i.e., $\Delta\omega \approx \Delta\varepsilon\partial\omega_m/\partial\varepsilon$, so that the right hand side has to be calculated for the unperturbed system. Reformulating this equation in terms of the refractive index n in $\mathcal{T}$, this results in equation (3):

$$\frac{\partial\omega_m}{\partial n} = -\omega_m n\int\limits_{\mathcal{T}} \mathrm{d}V\mathbf{E}_m^2(\mathbf{r})\,. \tag{S49}$$

Note that this equation can be used independently of the underlying geometry, provided that the modes are normalized correctly. The final result of the analytical normalization differs between different geometries, see [1–6]. For one- and two-dimensional periodic structures, we have derived here the correct analytical normalization, with the final result provided in equation (S34) and summarized in equation (3) of the main manuscript.

5 Relation to Purcell effect

We would like to emphasize that the correct mode normalization is also crucial for calculating the coupling of single emitters with nanoantennas. In the weak coupling regime, this interaction is described by the so-called Purcell factor [15], which states that the spontaneous emission rate of a dipole of frequency $\omega_\mathrm{d} \approx \mathrm{Re}(\omega_m)$ is approximately enhanced by

$$F = \frac{6\pi c^3 Q_m}{\omega_\mathrm{d}^3 V_m}\,, \tag{S50}$$

where $Q_m = |\mathrm{Re}(\omega_m)/2\mathrm{Im}(\omega_m)|$ is the quality factor of the resonance and V_m is the corresponding mode volume. As shown in [6], when reformulating the denominator on resonance as $\omega_d^2\mathrm{Re}(\omega_m V_m)$, this equation is still valid in the single mode approximation for the resonances of nanoantennas, provided that we normalize the resonant field distributions correctly and redefine the mode volume as

$$\frac{1}{V_m} = \left[\mathbf{e}_\mathrm{d}\cdot\mathbf{E}_m(\mathbf{r}_\mathrm{d})\right]^2\,. \tag{S51}$$

In this case, $\mathbf{r}_\mathrm{d}$ is the position of the dipole, and $\mathbf{e}_\mathrm{d}$ is the corresponding unit vector of its polarization. If the orientation of the dipole is not fixed, e.g., due to a random orientation of the dipole, we will have to average over the different orientations of the dipole. In particular, we may average over dipoles with polarization along the basis vectors $\mathbf{e}_x$, $\mathbf{e}_y$, and $\mathbf{e}_z$, resulting in the averaged Purcell factor

$$\langle F\rangle = \frac{F_x + F_y + F_z}{3} = \frac{2\pi c^3 Q_m}{\omega^3}\left[(\mathbf{e}_x\cdot\mathbf{E}_m)^2 + (\mathbf{e}_y\cdot\mathbf{E}_m)^2 + (\mathbf{e}_z\cdot\mathbf{E}_m)^2\right] = \frac{2\pi c^3 Q_m}{\omega^3}\mathbf{E}_m^2\,. \tag{S52}$$

With this result, we may now define the averaged mode volume as follows:

$$\langle V_m \rangle = \frac{3}{\mathbf{E}_m^2}\,. \tag{S53}$$

Thus, using this locally defined averaged mode volume, equation (S49) can be written as

$$\frac{\partial \omega_m}{\partial n} = -\omega_m n \int\limits_{\mathcal{T}} \mathrm{d}V \frac{3}{\langle V_m \rangle}\,, \tag{S54}$$

and the figure of merit (FOM) defined in equation (8) of the main manuscript becomes

$$\mathrm{FOM} = \left| \frac{1}{\mathrm{Im}(\omega_m)} \frac{\partial \omega_m}{\partial n} \right| \approx \left| 6n \int\limits_{\mathcal{T}} \mathrm{d}V \frac{Q_m}{\langle V_m \rangle} \right|. \tag{S55}$$

Hence, the FOM is proportional to the Purcell factor. Physically, it is clear that a high quality factor as well as a small mode volume is superior for increasing the spontaneous emission rate of a dipole, because it means that the lifetime of the resonance as the time of interaction between dipole and resonance is large and the local field is strongly enhanced. As the Purcell effect reflects the action of the nanoantenna on the dipole, it is not surprising due to reciprocity that the impact of the induced dipoles in the surrounding of a nanoantenna is strongest for the same conditions, i.e., the sensing performance is best for large field enhancements and high quality factors.

6 Derivation of eigenmodes

We are using a scattering matrix approach based on the Fourier modal method with matched coordinates [12, 16] in order to calculate the optical properties of the periodic nanoantennas numerically. The eigenmodes can be derived from the scattering matrix by different techniques [17, 18]. We are using here a modification of the resonant approximation scheme described in [18]. The ansatz is to approximate the scattering matrix S by a background term plus a finite number of poles for the resonances:

$$S(\omega) = S_{\mathrm{BG}}(\omega) + L(\omega I - \Omega_p)^{-1} R\,. \tag{S56}$$

In this case, the background term $S_{\mathrm{BG}}(\omega)$ should be assumed to change only slowly with ω. Furthermore, Ω_p is a diagonal matrix containing the finite complex poles ω_m, I is a unit matrix of the same size, and matrices L and R are constructed from the frequency independent resonant output and input vectors, respectively, associated with each mode [17]. Therefore, for the dimensions of S and Ω_p, $\dim S \geq \dim \Omega_p$.

Differentiating the approximate scattering matrix of equation (S56) with respect to ω yields:

$$S'(\omega) \approx -L(\omega I - \Omega_p)^{-2} R\,. \tag{S57}$$

Note that the derivative of the background term has been neglected, as it should vary only slowly with ω. Multiplying equation (S56) with the inverse of equation (S57) results in

$$\left[S'(\omega)\right]^{-1} S(\omega) \approx R^{-1}(\omega I - \Omega_p) R\,. \tag{S58}$$

This approximation is valid when being close enough to the poles so that the background contribution becomes negligible. Thus, one obtains a simple eigenvalue equation with $\omega - \omega_m$ as eigenfrequencies and the column vectors of R^{-1} as eigenvectors of $[S'(\omega)]^{-1} S(\omega)$ in the case that $\dim S = \dim \Omega_p$. If $\dim S > \dim \Omega_p$, we can use the same projection techniques as described in the appendix of [18] to construct an eigenvalue equation of smaller dimension.

For this purpose, let us assume that S' has not full rank, or that at least some singular values are close to zero. Then, we can make a singular value decomposition of S' such that

$$S' = U\Sigma V^\dagger\,, \tag{S59}$$

where Σ is a diagonal matrix with the singular values on its diagonal, and U and V are unitary matrices. We can construct an approximate form of S' by omitting all singular values smaller than a certain threshold and removing the corresponding columns in U and V. With these reduced matrices Σ_r, U_r, and V_r,

$$S' \approx U_r\Sigma_r V_r^\dagger\,, \tag{S60}$$

and we can derive an approximate eigenvalue problem for the poles with $\dim\Omega_p$ as

$$(\omega I - \Omega_p)\mathbf{v} = \Sigma_r^{-1}U_r^\dagger S V_r\mathbf{v}\,. \tag{S61}$$

The poles can then be found iteratively by starting with a guess value ω_m^0, calculating the eigenvalues $\omega_m^0 - \omega_m^1$, and using the frequency ω_m^1 for the next iteration. The procedure stops, when $|\omega_m^j - \omega_m^{j+1}|$ becomes sufficiently small.

In contrast to [18], we do not use here the second-order derivative of equation (S56), but rely on the assumption that we are close enough to the important poles with our guess values. While the second-order derivative scheme of [18] may be more accurate far away from the poles, it requires the numerically expensive calculation of the second-order derivative of the scattering matrix. According to our experience, especially for two-dimensional periodic systems, it is therefore more efficient to use our modification with first-order derivative or a combination of both schemes, where the second-order derivative is only calculated in the initial steps when the current value ω_m^j is further away from an actual pole ω_m.

7 Rod antenna system

The perturbation theory developed above is mathematically exact, but the outgoing boundary conditions require investigating certain geometries, for which the homogeneous top and bottom half-spaces provide some constraints. We would like to investigate now in detail, how the thickness of the cover layer influences the results, and how this affects a direct comparison with experimental results.

7.1 Measurements

For the comparison of our theory to experiment, we fabricated $100 \times 100\,\mu m^2$ sized arrays of nanoantennas, on a $10 \times 10 \times 0.5\,mm^3$ glass slide. The structures with a length of 340 nm, a width of 60 nm, and a periodicity of 700 nm in each direction, were defined by a standard electron-beam lithography process with positive resist (PMMA), followed by evaporation of a 2 nm Cr adhesion layer and a 40 nm film of gold. A subsequent lift-off procedure removed the unexposed resist and thus the gold in the areas around the structures.

Measurements were carried out using a custom-made microfluidic silicone cell, which features a 50 µm thick channel with inlet and outlet tubing. A constant flow of analyte solution (pure water, ethanol and propanol) was ensured by placing a reservoir above and the outlet in a beaker below the cell.

Transmittance spectra were recorded every 30 s for 10 min per analyte, using a Fourier-transform infrared spectrometer, extended by an infrared microscope. An infrared polarizer set the polarization of the incident light, and an aperture confined the beam to the structured area. Reference measurements for normalization were taken prior to every single sample measurement at a point next to the gold nanoantennas, i.e., through cell, analyte, and substrate. Averaged spectra are shown in figure S1 on the right.

To evaluate the shift of the resonance, we fitted a Fano lineshape to $1-T$, where T denotes the measured transmittance. The corresponding complex resonance frequencies are $194.4 - 14.7i\,(\pm 0.1)$ THz for water, $192.8 - 14.8i\,(\pm 0.1)$ THz for ethanol, and $191.8 - 14.7i\,(\pm 0.1)$ THz for propanol. The refractive indices have been extracted from Kedenburg et al. (water, ethanol) and Moutzouris et al. (propanol) [19, 20]. Thus, we can estimate the change of the real part of the resonance frequency per refractive index unit (RIU) as $-45\,(\pm 5)$ THz/RIU (from water to ethanol) and $-50\,(\pm 10)$ THz/RIU (from ethanol to propanol).

7.2 Comparison

Figure S1 shows numerical (a) and experimental (b) transmittance spectra for the periodic array of rod antennas and different materials in the cover layer. The incident electric field is linearly polarized along the long antenna axis. Blue color denotes water in the cover layer ($n = 1.3183$ at 195 THz), red is ethanol ($n = 1.3539$ at 193 THz), and black is propanol ($n = 1.3738$ at 192 THz). The cover layer thickness is several microns in experiment. In the numerical calculations, we either consider a cover layer of 650 nm thickness (thick lines) as in the main manuscript, or an infinite cover layer (thin lines), which cannot be used in the perturbation equation (S49). The difference in transmittance is small for these two numerical scenarios.

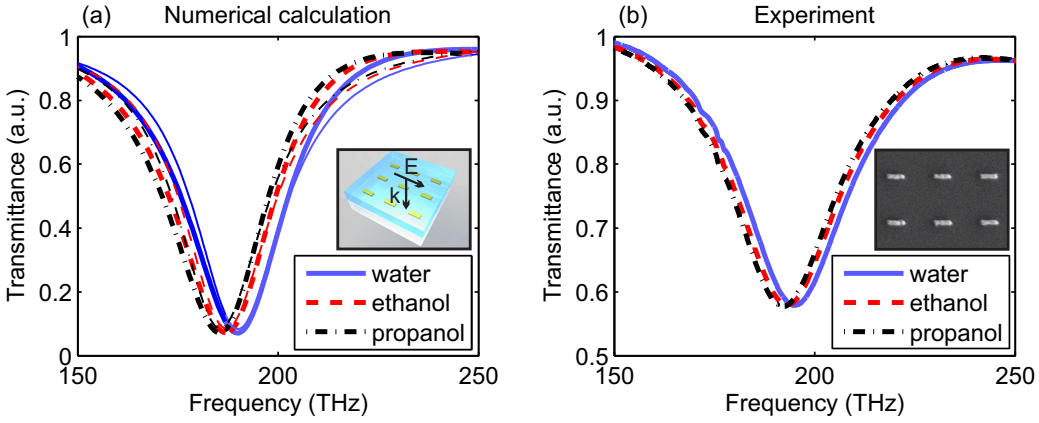

Figure S1: Numerical calculations (a) and experimental results (b) of the transmittance in the case of a periodic array of gold rod antennas for a normally incident plane wave polarized linearly along the long antenna axis. Colors denote different materials in the cover layer: water (blue, solid), ethanol (red, dashed), and propanol (black, dashed-dotted). Thick lines in the left panel depict the transmittance for a cover layer of 650 nm thickness, while thin lines have been obtained for an infinite half-space as cover layer. The thickness of the cover layer in experiment is several microns.

We observe in experiment and theory a reasonable agreement, but the spectral shift is smaller in experiment. There is also a difference in magnitude and linewidth between the experimental and the numerical results. This is a typical phenomenon and mostly originates in inhomogeneities due to fabrication tolerances in experiment. Furthermore, the fabricated antennas may exhibit a slightly different shape than the perfect cuboid of the numerical calculations, leading to different resonance linewidth and frequencies as well as modified near-field distributions. Another reason for deviations are pollutions of the liquids resulting in slightly different refractive indices.

To check the fitting procedure with the Fano lineshape, we applied this procedure to extract also the resonance positions from the numerically calculated spectra for 650 nm cover layer thickness, which provides some estimate of the accuracy of this procedure. The derived resonance frequencies are $190.7 - 13.8i\,(\pm 0.2)$ THz for water, $188.1 - 13.7i\,(\pm 0.2)$ THz for ethanol, and $186.6 - 13.7i\,(\pm 0.2)$ THz for propanol. The exact resonance frequencies directly

derived from Maxwell's equations are $191.0 - 15.4i$ THz for water, $188.5 - 15.4i$ THz for ethanol, and $187.2 - 15.3i$ THz for propanol. Hence, there is a deviation between the exact resonance frequencies and the fitted values that is larger than the tolerances of ± 0.2 THz provided from the fitting procedure. Although the resonance frequency shift per refractive index unit of roughly -73 THz/RIU derived from this fitting procedure is close to the -70 THz of the exact calculation, the results indicate an additional systematic error that might be due to a more complicated background contribution in the Fano lineshape due to close-by resonances. Therefore, it is in general difficult to estimate the resonance frequency shift per refractive index units from experimental and numerical spectra. However, it is reasonable to expect a qualitative agreement between experiment and theory in the sense that a sensitive resonance in theoretical calculations can be expected to be also very sensitive in experiments.

7.3 Cover layer thickness

It is clear that our system with 650 nm cover layer is not equivalent to the experimental realization with several microns thickness. The experimental measurements using the Fano fit to determine the shift of the resonance position indicate smaller absolute values than the theoretical values of the perturbation theory. In order to get a better understanding of the influence of the cover layer, we thoroughly investigated the resonance frequency and linewidth in dependence of the cover layer thickness and studied also the corresponding behavior of the shifts predicted from equation (S49), see figure S2.

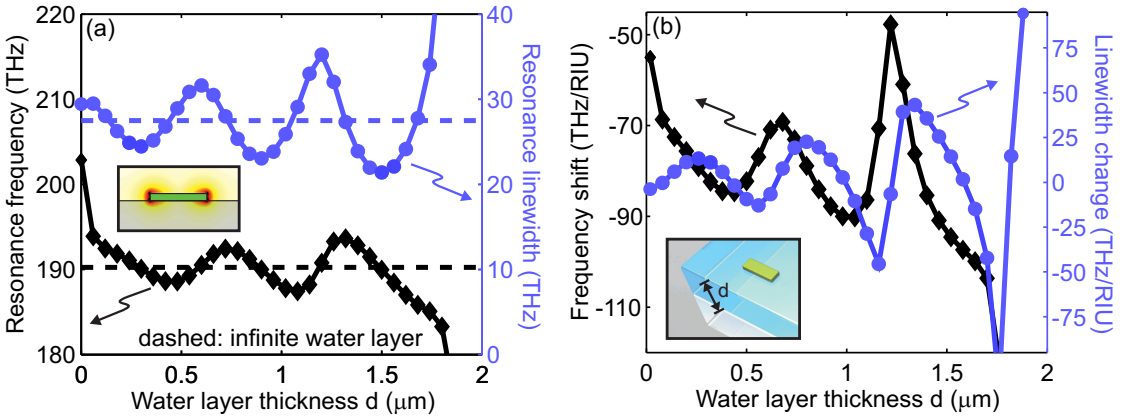

Figure S2: (a) Dependence of resonance position (black) and resonance linewidth (blue) on the thickness of the cover layer. Dashed lines denote an infinite thickness. We observe a strong shift for small thicknesses, after which the resonance position and linewidth start to oscillate around the values for infinite thickness due to constructive and destructive interference in the cover layer. For large thickness around 1.5 µm, influences of Fabry-Perot modes become visible, resulting in much stronger deviations. (b) Corresponding resonance shifts per refractive index unit as predicted from equation (S49) for small changes of the refractive index in the cover layer.

The resonance frequency (black, diamonds) and the resonance linewidth (blue, circles) in figure S2a have been derived for water cover layers between 0 µm and 2 µm thickness (solid lines) as well as for an infinite cover layer (dashed lines). For thicknesses below 1.5 µm, the resonance frequency and linewidth oscillate around the results for the infinite cover layer. At larger thicknesses, the deviations become significant. The reason is the formation of Fabry-Perot modes in the cover layer, which couple to the plasmonic modes. As the quality factor for these Fabry-Perot modes is rather low due to the small index contrast between air and the cover layer, this coupling results in an increase of the resonant linewidth (see blue line with circle), accompanied by a drift of the resonance frequency to lower values (black diamonds). Note that there are no Fabry-Perot modes formed in experiment, as the top

surface is rather rough and scatters light in all directions, countervailing the constructive interference of multiple reflections at the top and bottom interfaces.

The corresponding predictions of the perturbation equation (S49) can be seen in figure S2b. Evidently, there are similar fluctuations as in the case of the resonance frequencies, which become larger for larger thicknesses. In principle, any resonance shift between $-50\,\mathrm{THz}$ and $-120\,\mathrm{THz}$ is possible in that thickness range. For the main manuscript, we have not selected the thickness with the best agreement to the experiment, because firstly, we do not want to raise expectations that the perturbation theory cannot fulfill due to the above mentioned deviations between theory and experiment. Secondly, the calculation of the field distributions becomes more memory consuming for larger cover layer thicknesses, thus being less efficient. Thirdly, the onset of the Fabry-Perot modes is even at smaller thicknesses for the other examples in the main manuscript. Therefore, we selected the 650 nm thickness, as it is thick enough to cover the near-field region and thin enough to avoid Fabry-Perot modes. Moreover, it provides us for all examples a resonance frequency that is similar to the system with infinite cover layer thickness.

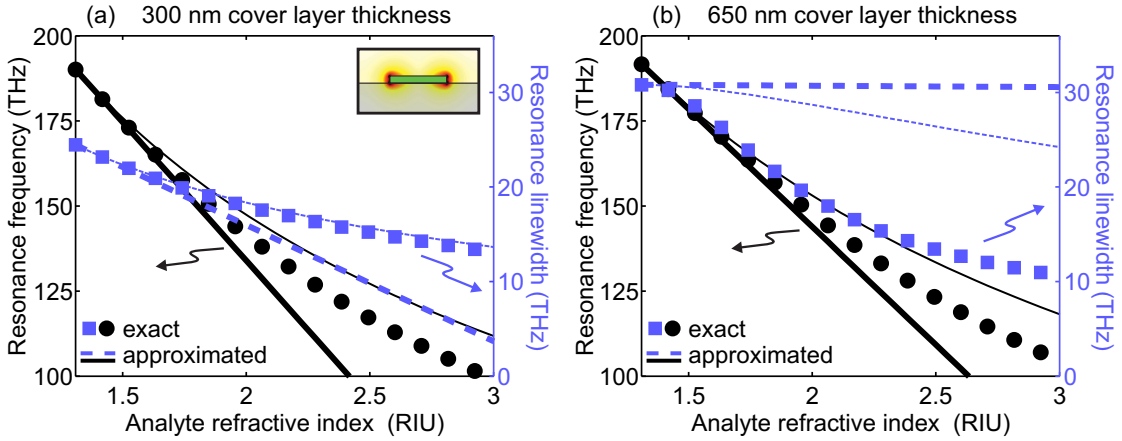

Figure S3: Refractive index dependence of the exact resonance frequency (black circles) and the resonance linewidth (blue squares) in comparison with the resonance frequency (black sold lines) and the resonance linewidth (blue dashed lines) of the perturbation theory as defined in equation (S46) (thin lines) as well as the linear equation (S49) (thick lines) for a cover layer thickness of (a) 300 nm and (b) 650 nm.

Finally, we investigate also the exact dependence of resonance frequency and linewidth for larger ranges of refractive indices between $n = 1.31$ and $n = 3$ for different cover layer thicknesses and compare it to the linear dependence obtained from the perturbation theory. As it can be seen in figure S3, the exact results exhibit a linear dependence on the refractive index for small deviations from $n = 1.31$ for the cover layer thicknesses of (a) 300 nm (b) and 650 nm, which is reproduced well by the perturbation theory. Note that thin lines correspond to the more precise formulation of equation (S46), whereas thick lines have been calculated by the linearized formulation of equation (S49). Further away from $n = 1.31$, we observe a quadratic deviation of the exact results from the perturbation theory. Except for the resonance linewidth in figure S3b, the deviation is negligible up to $n \approx 1.7$. Regarding the resonance linewidth in figure S3b, the initial slope of the exact results and the perturbation theory is close to zero, indicating an extremal situation, in which the quadratic dependence becomes dominant. The extremal situation can be also seen in figure S2a, where we see that the resonance linewidth is close to a maximum at a water layer thickness of 650 nm. Therefore, we are in the situation of a minimum quality factor, and any structural deviation must immediately result in a reduction of the linewidth. Finally, it is worth mentioning that

the approximate equation (S46) provides a better agreement with the exact result than the linearized equation (S49), especially when considering the resonance linewidth in figure S3a.

References

[1] E. A. Muljarov, W. Langbein, and R. Zimmermann, Brillouin-Wigner perturbation theory in open electromagnetic systems, Europhys. Lett. **92**, 50010 (2010).

[2] M. B. Doost, W. Langbein, and E. A. Muljarov, Resonant-state expansion applied to planar open optical systems, Phys. Rev. A **85**, 023835 (2012).

[3] M. B. Doost, W. Langbein, and E. A. Muljarov, Resonant state expansion applied to two-dimensional open optical systems, Phys. Rev. A **87**, 043827 (2013).

[4] M. B. Doost, W. Langbein, and E. A. Muljarov, Resonant-state expansion applied to three-dimensional open optical systems, Phys. Rev. A **90**, 013834 (2014).

[5] L. J. Armitage, M. B. Doost, W. Langbein, and E. A. Muljarov, Resonant-state expansion applied to planar waveguides, Phys. Rev. A **89**, 053832 (2014).

[6] E. A. Muljarov and W. Langbein, Exact mode volume and Purcell factor of open optical systems, arXiv:1409.6877v3 [cond-mat.mes-hall] (2014).

[7] H. M. Lai, P. T. Leung, K. Young, P. W. Barber, and S. C. Hill, Time-independent perturbation for leaking electromagnetic modes in open systems with application to resonances in microdroplets, Phys. Rev. A **41**, 5187–5198 (1990).

[8] C. Sauvan, J. P. Hugonin, I. S. Maksymov, and P. Lalanne, Theory of the spontaneous optical emission of nanosize photonic and plasmon resonators, Phys. Rev. Lett. **110**, 237401 (2013).

[9] Q. Bai, M. Perrin, C. Sauvan, J. P. Hugonin, and P. Lalanne, Efficient and intuitive method for the analysis of light scattering by a resonant nanostructure, Opt. Express **21**, 27371–27382 (2013).

[10] G. B. Arfken and H. J. Weber, *Mathematical methods for physicists*, Elsevier, London, 6th edition, 2011.

[11] T. Weiss, G. Granet, N. A. Gippius, S. G. Tikhodeev, and H. Giessen, Matched coordinates and adaptive spatial resolution in the Fourier modal method, Opt. Express **17**, 8051–8061 (2009).

[12] S. Essig and K. Busch, Generation of adaptive coordinates and their use in the Fourier modal method, Opt. Express **18**, 23258–23274 (2010).

[13] R. G. Barrera, G. A. Estévez, and J. Giraldo, Vector spherical harmonics and their application to magnetostatics, Eur. J. Phys. **6**, 287–294 (1985).

[14] E. A. Muljarov and W. Langbein, Resonant-state expansion of dispersive open optical systems: Creating gold from sand, Phys. Rev. B **93**, 075417 (2016).

[15] E. M. Purcell, Spontaneous emission probabilities at radio frequencies, Phys. Rev. **69**, 681 (1946).

[16] T. Weiss, N. A. Gippius, S. G. Tikhodeev, G. Granet, and H. Giessen, Efficient calculation of the optical properties of stacked metamaterials with a Fourier modal method, J. Opt. A: Pure Appl. Opt. **11**, 114019 (2009).

[17] T. Weiss, N. A. Gippius, S. G. Tikhodeev, G. Granet, and H. Giessen, Derivation of plasmonic resonances in the Fourier modal method with adaptive spatial resolution and matched coordinates, J. Opt. Soc. Am. A **28**, 238–244 (2011).

[18] D. A. Bykov and L. L. Doskolovich, Numerical methods for calculating poles of the scattering matrix with applications in grating theory, J. Lightwave Technol. **31**, 793–801 (2013).

[19] S. Kedenburg, M. Vieweg, T. Gissibl, and H. Giessen, Linear refractive index and absorption measurements of nonlinear optical liquids in the visible and near-infrared spectral region, Opt. Mater. Express **2**(11), 1588–1611 (2012).

[20] K. Moutzouris, M. Papamichael, S. Betsis, I. Stavrakas, G. Hloupis, and D. Triantis, Refractive, dispersive and thermo-optic properties of twelve organic solvents in the visible and near-infrared, Applied Physics B **116**(3), 617–622 (2014).